TISSUE ENGINEERING: Part A
Volume 18, Numbers 7 and 8, 2012

DOI: 10.1089/ten.tea.2011.0307

The Effect of Nano-Scale Topography on Keratinocyte Phenotype and Wound Healing Following Burn Injury

Leigh G. Parkinson, Ph.D.,[1–3] Suzanne M. Rea, FRCSI,[1,2,4,5] Andrew W. Stevenson, BSc(Hons),[1,2] Fiona M. Wood, FRACS,[1,2,4,5] and Mark W. Fear, Ph.D.[1,2,6]

Topographic modulation of tissue response is an important consideration in the design and manufacture of a biomaterial. In developing new tissue therapies for skin, all levels of architecture, including the nanoscale need to be considered. Here we show that keratinocyte phenotype is affected by nanoscale changes in topography with cell morphology, proliferation, and migration influenced by the pore size in anodic aluminum oxide membranes. A membrane with a pore size of 300 nm, which enhanced cell phenotype *in vitro,* was used as a dressing to cover a partial thickness burn injury in the pig. Wounds dressed with the membrane showed evidence of advanced healing with significantly less organizing granulation tissue and more mature epidermal layers than control wounds dressed with a standard burns dressing. The results demonstrate the importance of nanoscale topography in modulating keratinocyte phenotype and skin wound healing.

Introduction

Burns are one of the most devastating injuries encountered in medicine, and delayed treatment can lead to excessive scarring that can have profound physical and psychological effects on the patient. New tissue engineering technologies are focused on providing fast wound closure to limit scar formation, with the effect of topography on cell phenotype receiving considerable attention.

Topographic modulation of tissue response is an important consideration during the design and manufacture of a biomaterial. The ability to direct and guide cell behavior has long been established with micron-sized features,[1–5] and it is rapidly becoming apparent that nano-scale topography may be of great importance when considering how cells respond to their environment.[6–12] In developing new therapies for skin wound healing, it is important to understand and potentially exploit the effects of nano-scale topography on keratinocyte phenotype to ultimately provide a device that will improve wound healing and the quality of the scar.

Previous work by our group detailed the fabrication of large-scale, highly reproducible nanoporous anodic aluminum oxide (AAO) membranes with a range of pore sizes for their potential use in skin tissue engineering.[13] Preliminary experiments showed that keratinocytes adhered to the membranes and were sensitive to nano-scale changes in topography. In this work, detailed studies of cell phenotype on the nanoporous membranes are presented and discussed with an optimal pore size determined for application *in vivo*. AAO membranes were used as an interactive dressing to treat deep dermal partial thickness burns in a porcine model[13,14] to exploit the effects of the membranes observed on cell phenotype *in vitro*. The data suggests that AAO membranes and nano-scale topography have potential for further application in skin wound repair.

Materials and Methods

Nanoporous AAO membranes

Large scale, highly reproducible nanoporous AAO membranes were prepared and characterized as previously described.[13] Four membranes with different pore sizes were fabricated using different anodizing conditions (Table 1). Pore size geometry was assessed using Scanning Probe Image Processor (SPIP) software (version 5.1.2, Image Metrology, Denmark).

Keratinocyte morphology studies on nanoporous membranes

The HaCaT cell line was used for all cell experiments and maintained as previously described.[13] Cell morphology and

[1]McComb Research Foundation, Perth, Australia.
[2]The University of Western Australia, Burn Injury Repair Unit, School of Surgery, Perth, Australia.
[3]Murdoch University, School of Engineering and Energy, Perth, Australia.
[4]Royal Perth Hospital, Perth, Australia.
[5]Princess Margaret Hospital, Perth Australia.
[6]Notre Dame University, School of Medicine, Perth, Australia.

Table 1. Anodizing Conditions for the Fabrication of AAO Membranes with Different Pore sizes

Anodizing Acid	*Voltage*	*Time of 1° anodization (h)*	*Time of 2° anodization (h)*
Sulfuric acid (0.3 M)	24	5	5
Oxalic acid (0.3 M)	30	7	14
Oxalic acid (0.3 M)	60	4	4
Phosphoric acid (0.3 M)	130	5	7

AAO, anodic aluminum oxide.

interaction with the prepared membranes was studied using scanning electron microscopy (SEM). Membranes were cut into 12 mm circular discs and fixed to sterile 12 mm circular glass coverslips with a small amount of silicone adhesive at one end. The samples were then placed in 24-well cell culture plates and UV-sterilized for 1 h. HaCaT cells were seeded on the membranes at a density of 5×10^4 cells/mL in 24-well plates at a volume of 1 mL/well, and were incubated at 37°C with 5% carbon dioxide (CO_2) for 12 h. Cells were also seeded on glass coverslips as a control. Preparations were fixed and processed for SEM using a microwave-assisted technique, which allowed for faster processing and better preservation of fine structural detail.[15,16] Samples were critical point dried from ethanol, mounted on aluminum stubs with carbon tape and paint, sputter coated with gold, and analyzed under a Zeiss 1555 variable-pressure scanning electron microscope.

Keratinocyte proliferation and migration on nanoporous membranes

Keratinocyte proliferation was quantified over 3 days of culture on each of the prepared membranes using a standard 3-(4,5-dimethylthiazol-2-yl)-5-(3-carboxymethoxyphenyl)-2-(4-sulfophenyl)-2H-tetrazolium, innersalt (MTS) cell proliferation assay (Promega, Madison, WI), as per manufacturer's instructions. Triplicate samples of the membranes were cut to an exact size to completely cover the bottom of the wells of 96-well plates and UV-sterilized for 1 h before washing with fresh media. HaCaT cells were seeded at 2.5×10^4 cells/mL in 100 μL volume per well and at 0, 24, 48, and 72 h, samples were treated with CellTiter 96® AQ_{ueous} One solution and incubated for 3 h at 37°C and 5% CO_2.[17] The absorbance of the resulting supernatant solutions was read at 490 nm to determine cell number. All assays had a minimum of three replicates and were repeated to ensure reproducibility.

Keratinocyte migration across the surface of the membranes was measured using a modified version of the scratch assay. Triplicate membrane samples of the prepared membranes were cut to an exact size to cover the bottom of 12-well plates and adhered with a small amount of silicone glue at one end of the well. Plain glass microscopy slides (0.98 mm thick) were cut to fit the center of the wells and were stood upright and secured to provide a barrier to cell growth and thus a cell free area for analysis of cell migration. HaCaT cells were labeled with an optimal concentration of 10 μM CellTrace carboxyfluorescein succinimidyl ester (CFSE; Invitrogen Molecular Probes, Eugene, OR) to allow visualization of cells on the opaque membranes by fluorescent microscopy. Cells were seeded at a density of 2×10^5 cells/mL at a volume of 1 mL/well to the prepared plates and incubated at 37°C with 5% CO_2. Once the cell monolayer was confluent (~48 h), the glass barriers were removed to reveal a cell-free area through the middle of the well. The media was aspirated and the wells were washed with phosphate buffered saline (PBS) before being replaced with fresh media and returned to the incubator. The media was changed every 12 h to allow clear observation of the cells. Cell migration was monitored by population of the cleared area with cells over time. Photographs of the middle of the well were taken immediately after the removal of the glass barriers using a light microscope fixed with a 488 nm excitation source (Nikon Eclipse Inverted Microscope V1.21, final objective ×4). The fields were marked, and the same fields were photographed again at 12, 18, 24, 30, 36, 42, 48, and 60 h later. The residual gap between the migrating keratinocytes was measured using ImageJ software[18] and the results were expressed as a percentage of cell coverage by comparison with $t=0$ h. Control wells with no nanomembrane were also included. All assays had a minimum three replicates and were repeated to ensure reproducibility.

Animals

All animal work was approved by the institutional animal ethics committee (University of Western Australia, Perth, Australia; Permit number: RA/3/100/866) and was performed in accordance with the National Health and Medical Research Council Australian Code of Practice for the Care and Use of Animals for Scientific Purposes (seventh edition). Large, white, female juvenile pigs of 16–22 kg were used for the study ($n=8$).

Animal surgery

Anesthesia was induced with an intramuscular (IM) dose of 4.4 mg/kg zoletil and 2.2 mg/kg xylazine and maintained with isoflurane via endotracheal intubation. The hair on the back and flanks was clipped, and the proposed wound area was carefully shaved. The whole area was thoroughly washed with clean water, and surgical iodine was applied prior to wounding. Buprenorphine (0.02 mg/kg) was administered as an analgesic on induction. Wounds were created using hot water in a Pyrex laboratory Schott Bottle (500 mL) that had the bottom removed and replaced with cling wrap as described previously.[14] Once the water was at the desired temperature of 92°C, it was placed on the dorsal flank of the pig for 15 seconds to create a deep dermal partial thickness injury.[14] Two burns were created on each animal, one on each flank (in matched positions), with the device being held in place by the same person for the required time (total wounds $n=16$). Wounds were photographed alongside a ruler using a Panasonic Lumix DMC-FS42 digital camera before being dressed. Carprofen (4 mg/kg) and Fentanyl patches (75μg/h) were administered following the burn injury, with the patches replaced at days 3 and 7 post burn.

Wound dressings

On each pig, one wound was dressed as "control," and the other was dressed as "test" with the nanoporous membrane. Control wounds were dressed with Acticoat and gauze and held to the pig with Fixomull ($n=8$). Test wounds were dressed with 300 nm membranes (that had been previously

autoclaved) and then Acticoat, gauze and Fixomull ($n=8$). Tubigrip stocking was placed over the whole pig to ensure dressings were held in place. To protect the wound areas, custom made vinyl garments were fastened to the pigs with Velcro and straps. The garments were semi waterproof and were vital in securing the dressings and keeping the whole wound areas clean.

Dressing changes and biopsy collection

At days 7, 14, 21, 42, 56, and 70 post-burn, animals were sedated with an IM dose of ketamine/xlyazine (16 mg/kg ketamine/2.2 mg/kg xylazine) for dressing changes and/or wound examination. Dressings were carefully removed. The wounds were examined and photographed, and a clinical description was noted. Also while sedated, punch biopsies were taken from both wounds (control and test) of three pigs at all time-points to gain histological data of the wound depth and the healing process over time. Following a subcutaneous injection of local anesthetic (1% Lignocaine, 2 mL), a 6 mm punch biopsy was taken 2 cm from the edge of the wound. Care was taken to evenly spread the biopsy sites from week to week. Biopsies of uninjured, normal skin were also collected and processed for comparison. The remaining five pigs did not have biopsies collected, which allowed the wounds to heal without repeated insult.

The wounds were re-dressed with the appropriate dressings (i.e., control or test) until day 21 post burn, by which time all wounds were completely re-epithelialized. To protect the maturing wounds, gauze, Fixomull, and the vinyl garments were applied until day 42 post burn. For the remainder of the study, all protective dressings and garments were removed. In an effort to alleviate pruritis of the scars, the affected areas were washed and moisturized every 2 days.

Blood collection and analysis

At the time of injury, day 7, and day 14 post burn, blood was collected from a prominent ear vain of three pigs for trace metal analysis of aluminum. Blood was collected into Vacutainer® tubes (containing ethylenediaminetetraacetic acid [EDTA]; anticoagulant), and centrifuged (3000 rpm, 10 min) to separate the red blood cells from the plasma. Plasma was collected and stored at −80°C before further analysis. Samples were analyzed commercially by a National Association of Testing Authorities accredited laboratory using inductively coupled plasma-atomic emission spectroscopy (ICP-AES). Aluminum was detected at a limit of 0.05 mg/L.

Euthanasia and scar excision

Four animals were euthanized at day 56, and four at day 70 post burn, with sodium pentobarbitone (Lethabarb). The wounds were photographed, and a blinded clinical assessment of the scar was recorded by an experienced burns surgeon. The entire wound area plus 0.5 cm of surrounding skin was excised and fixed in 10% formal saline for processing. Normal, uninjured skin (close to the wounded sites) was also excised and processed for comparison.

Tissue preparation

All tissue samples were fixed in 10% formal saline for 24 h at 4°C, washed in phosphate buffered saline (PBS) and then processed through alcohol/toluene/paraffin wax. Excised scars were cut through the middle and two samples per wound were processed for sectioning along both the anteroposterior and dorsoventral axes. Three sections (5 μm) from each sample were collected for histological staining and analysis.

Histology

Of the three sections collected from each sample, two were stained with haematoxylin and eosin (H&E) and mounted in distyrene, di-N-butylphthalate, xylene for histological analysis. The remaining section was stained with Masson's trichrome to further examine collagen morphology in the scarred tissue. Each whole section was captured using an Aperio Scanscope digital slide scanner fitted with a 40× objective. Images were processed, analyzed, and representative snapshots of the sections were captured using the associated software, Aperio ImageScope v 10.1.3.2028 (Aperio Technologies).

Wound-healing assessments: gross morphology and histological analysis

Gross re-epithelialization was quantified at each time point in a blinded manner by digital planimetry of the collected photographs using Advanced Wound Assessment and Measurement System software (Savant Imaging, 2009). Areas of re-epithelialization were traced and the results were expressed as a percentage of re-epithelialization by comparison with the original burn area. At least two photographs of each wound, taken in different orientations, were analyzed to ensure accurate results.

Upon euthanasia, blinded clinical assessments of the scars were recorded on site by an experienced burns clinician. The assessments were judged based upon the Vancouver Scar Scale (VSS).[19]

All histological analyses were performed in a blinded fashion. All stained skin sections were analyzed electronically using Aperio ImageScope v 10.1.3.2028 software (Aperio Technologies). General observations pertaining to skin architecture, and the maturation and organization of dermal collagens were noted. For each section, total skin thickness (epidermis and dermis) and epidermal thickness were measured, and the amount of organizing granulation tissue (OGT) as a percentage of the dermis was determined.[14,20] The results from each section of a single wound were collated. For example, for each of the final excised scars, the results are expressed as the average of all six sections collected from the wound (i.e., from both anteroposterior and dorsoventral axes).

Statistics

Results were analyzed using the statistical package StatView for Windows (SAS Institute Inc. Cary, NC) and SPSS (IBM Corporation). The linear mixed model[21] was used to analyze the proliferation and migration data, with significant differences indicated by $p<0.05$. For the in vivo studies, paired student's t-tests were used to determine statistically significant differences between treatments at the various time-points, using the means for control and test on each pig as the paired data. Significance was indicated by $p<0.05$.

Results

Anodic aluminum oxide membranes

Large scale, highly reproducible nanoporous AAO membranes were prepared and characterized as previously described.[13] Representative SEM images of each of the prepared membranes are shown in Figure 1. Pore geometry was analyzed using SPIP software over full SEM micrographs and also within ordered pore domains. A summary of pore geometries of prepared AAO membranes is given in Table 2.

SEM study of keratinocyte cell morphology on nanoporous AAO membranes

HaCaT cells cultured on glass (control surface) were mostly well spread with small membrane protrusions (Fig. 2A, B). Cells were covered with numerous microvilli, and both sheet-like lamellipodium and spike-like filopodium were observed (Fig. 2B).

HaCaT keratinocyte cell morphology was also characterized on each of the prepared AAO membranes. On all membranes, cell attachment was observed across the whole surface of the prepared samples (as evident from Fig. 2C, E, G, I) and distributed homogeneously in a manner similar to the glass coverslips. At higher magnifications, microvilli were observed on the cell surfaces, together with many filopodia projecting from the cell membranes over the nanoporous surfaces. On the 41 nm membrane, cells mostly had a rounded morphology (Fig. 2C) and produced many long and short filopodia to explore the AAO substrate (Fig. 2D). Flat and spread cells were also present on the membrane, with clear lamellipodia and filopodia extending from the cell body. The filopodia (approximately 60 nm diameter) were larger than the size of the pores and appeared to lie across the surface of the membrane. Similar observations were recorded with keratinocytes cultured on membranes with a pore size of 58 nm (Fig. 2E–F) and 114 nm, with the filopodia appearing to penetrate into the pores of the underlying substrate (Fig. 2G–H). These images show a direct interaction of keratinocyte with the nanoporous topography with many filopodial/pore interactions.

In contrast to the other membranes, cells on the 300 nm membrane were notably more spread and flat, with a similar morphology to cells on the glass cover slips (Fig. 2I). However, cells still projected many filopodia that were able to directly interact with the pores, appearing to penetrate the surface of the membrane as with the 114 nm membrane (Fig. 2J).

Keratinocyte proliferation and migration on nanoporous AAO membranes

Cell proliferation was quantified on each of the prepared nanoporous membranes, with results showing an effect of nano-scale topography on cell growth (Fig. 3A). In summary, there was no significant difference in the rate of change for the 300 nm membrane (72 h; 0.620 ± 0.017) compared to the control (0.647 ± 0.008), with both supporting the fastest cell proliferation ($p = 0.714$). However, the rate of change for proliferation was significant for all other membranes when compared to the control, indicating slower proliferation ($p < 0.006$).

Keratinocyte migration was analyzed by population of cells into a cell free area on the nanoporous substrates over time. Each of the membranes were prepared for analysis, however the 114 nm membrane was too thick/opaque to allow clear and accurate observation of cells on its surface and was therefore excluded from analysis. All remaining pore sizes and the control were characterized for their effect on migration. There was an effect due to nanotopography on cell motility, with cells migrating fastest across the 300 nm

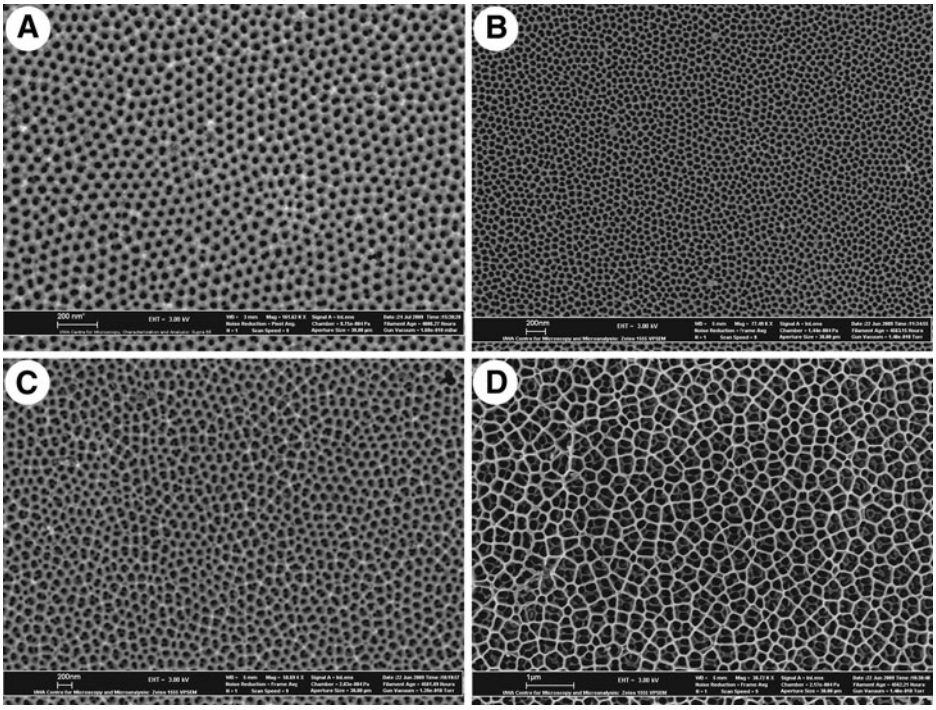

FIG. 1. Scanning electron microscope (SEM) images of prepared anodic aluminium oxide (AAO) membranes. **(A)** Membrane prepared in sulfuric acid at 24 V, pore size 41 nm. (**B**) Membrane prepared in oxalic acid at 30 V, pore size 58 nm. (**C**) Membrane prepared in oxalic acid at 60 V, pore size 114 nm. **(D)** Membrane prepared in phosphoric acid at 130 V, pore size 300 nm.

Table 2. Summary of Pore Geometries of Prepared AAO Membranes

	Overall pore geometry				*Pore geometry within ordered domains*		
Membrane	*Pores/ μm*	*Pore diameter (nm)*	*Maximum calibre (nm)*	*Interpore distance (nm)*	*Pore diameter (nm)*	*Maximum calibre (nm)*	*Interpore distance (nm)*
Sulfuric acid 24 V	280 ± 9	41 ± 4	47 ± 7	58 ± 4	40 ± 2.5	44 ± 4	58 ± 3
Oxalic acid 30 V	194 ± 7	58 ± 7	66 ± 11	68 ± 6	54 ± 3	58 ± 4	68 ± 3
Oxalic acid 60 V	48 ± 2	114 ± 14	130 ± 24	137 ± 10	114 ± 4	123 ± 6	141 ± 6
Phosphoric acid 130 V	10 ± 1	300 ± 79	360 ± 91	277 ± 38	No ordered domains		

membrane compared to the control and all other membranes tested (Fig. 3B). Statistical analysis showed there was a significant difference in the rate of change for migration for the 300 nm membrane (42 h; 100%) compared to the control (91.0 ± 1.1%) ($p = 0.001$). There was no significant difference between the 41 nm (93.2 ± 1.6%) and 58 nm (84.0 ± 4.6%) membranes compared to the control ($p = 0.642$, $p = 0.087$ respectively). However to the first 30 h, there was a trend of faster cell migration across all of the membranes tested compared to the control (Fig. 3B).

Overall, the 300 nm membrane performed optimally in the *in vitro* studies, supporting similar proliferation and faster migration when compared to the control, and both increased proliferation and migration over the other membranes tested. This membrane had the effects on keratinocyte phenotype that would be most beneficial in the context of wound repair and was therefore selected for application *in vivo.*

Animals and membranes

The average pig weight at time of burn injury was 19.6 ± 1.9 kg (mean ± SD) and increased to 54.9 ± 4.2 kg at day 70 post-burn when animals were euthanized. Animal weight gain was steady and linear suggesting no adverse effects of the burn injuries or treatment on animal welfare. Autoclaved 300 nm membranes were applied to the wound bed with the remaining aluminum substrate left on the backside of the membrane to provide extra mechanical support. There was no observed degradation of the membranes at dressing changes and there was no incidence of infection or adverse events.

Characterization of the burn injury and wound healing

The average burn area was 53.9 ± 0.7 cm^2 (mean ± SE). The size of the membrane was 56 cm^2 (supported by the aluminum substrate of 71 cm^2), which completely covered the wounded area and allowed gluing of the dressing around the edge so that it remained in place. Burn wounds were characterized by a white, nonblanching area, with a red hyperemic zone around the wound border (Fig. 4A, B). The progression of wound healing for both control and membrane treated wounds for one of the pigs can be seen in Figure 4. Islands of re-epithelialization were seen by day 7, as well as from the wound edges, with further epithelial coverage by day 14 (data not shown). Gross morphology of healing wounds was similar for both control and membrane treated sites. Complete re-epithelialization was seen for all wounds by day 21 (Fig. 4C, D). As a result, all primary dressings were removed at day 21; however, the newly formed and still fragile epidermis was protected with plain gauze, Fixomull, and the protective jackets until day 42 post burn. By day 56, slightly contracted and purple scars were observed for both wounds, which continued to mature to mostly flat scars by day 70 when animals were euthanized (Fig. 4E, F). Histology showed that wounds were re-epithelialized by day 21 and there were no signs of infection in any of the biopsies. By day 42, there was massive hypertrophy of the dermis, with the organizing granulation tissue (OGT) prominent (data not shown).

Gross re-epithelialization

Overall, there was no significant difference in gross re-epithelialization between control and membrane treated wounds at any of the time-points (Fig. 5A). Re-epithelialization at day 7 post burn was 53 ± 14% (mean ± SE) for control wounds and 66 ± 10% for membrane treated wounds (paired t-test, p = 0.4315). By day 14, control wounds were 93 ± 4% re-epithelialized, and membrane wounds 97 ± 2 % re-epithelialized (paired t-test, p = 0.3687). All wounds were completely (100%) re-epithelialized by day 21 post burn.

Blood

To assess membrane stability and detect any systemic absorption of aluminum from the membranes, blood samples were collected preinjury and at days 7 and 14 post burn and analyzed for total aluminum content by ICP-AES. Overall, there was no difference in the amount of total aluminum from pre- and postmembrane blood samples (paired *t*-test, day 0 to day 7; $p = 0.6549$) (Fig. 5B).

Final scar outcomes

The final scars were assessed by an experienced clinician who was blinded to the treatment at each site. Scars were judged based upon a modified version of the Vancouver Scar Scale (VSS) and general observations (Fig. 6A). Overall, there was no significant difference between the final scar scores from control (3.25 ± 0.5 /11) and membrane (3.56 ± 0.7 /11) treated wounds (paired *I*-test, $p = 0.277$). Scars were mostly pale purple in color, which was consistent for both control and membrane treated wounds (average vascularity score, 2.25 ± 0.4 /3 for both treatments). The final scars were also very pliable and supple (control 0.88 ± 0.1 /5 vs. membrane 1.06 ± 0.2 /5) and mostly flat (control 0.125 ± 0.125 /3 vs. membrane 0.25 ± 0.2 /3).

Total skin thickness

The thickness of the epidermis and dermis was measured histologically using sections and the data presented shows the paired results from the test and control sites on each

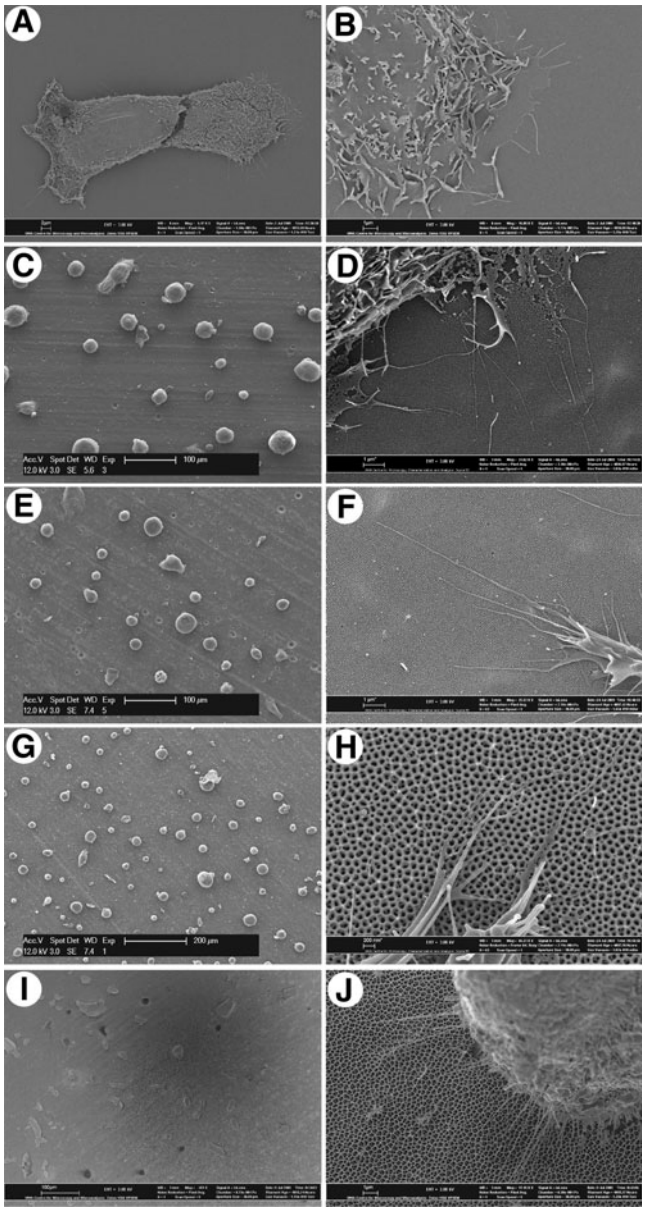

FIG. 2. SEM images of keratinocytes grown on: **(A, B)** Flat glass control surface (scale bars [SB]: 2 μm, 1 μm). **(C, D)** 41 nm membrane (SB: 100 μm, 1 μm). **(E, F)** 58 nm membrane (SB: 100 μm, 1 μm). **(G, H)** 114 nm membrane (SB: 200 μm, 200 nm). **(I, J)** 300 nm membrane (SB: 100 μm. 1 μm). Cells produced many filopodia to explore the nanoporous substrate and had a mostly rounded morphology on the 41 nm, 58 nm, and 114 nm membranes. However, on the control and 300 nm membrane, cells had a more flat and spread morphology.

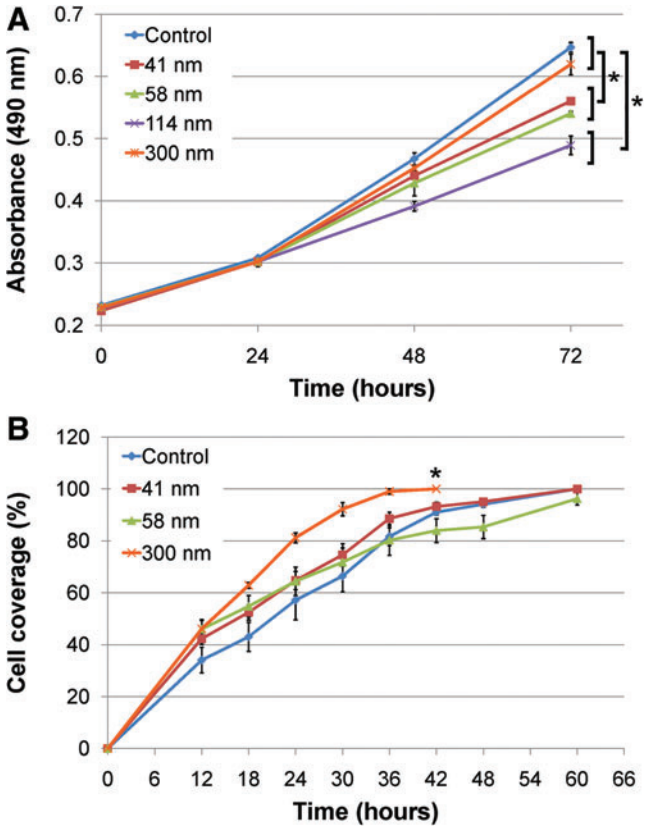

FIG. 3. Keratinocyte proliferation and migration on the prepared AAO membranes. **(A)** There was no significant difference between the control and 300 nm membrane, with both supporting the fastest cell proliferation. There was significantly less proliferation on all other membranes. Values are the mean absorbance of three replicates ± SE (*$p < 0.05$ as significant). **(B)** Cell migration was significantly faster across the 300 nm membrane compared to the control and the other membranes. There was no difference in the rate of change for migration for the 41 and 58 nm membranes compared to the control. Values are the mean of three replicates ± SE (*$p < 0.05$ as significant). Color images available online at www.liebertonline.com/tea

individual pig ($n = 4$ euthanized at day 56; $n = 4$ euthanized at day 70; Fig. 6B). Regardless of the day euthanized, skin from both control and membrane treatment groups was significantly thicker than normal uninjured skin (3.57 ± 0.10 mm; unpaired *t*-tests, $p < 0.05$). There was no significant difference in the average skin thickness between day 56 (4.91 ± 0.31 mm) and day 70 (4.56 ± 0.10 mm) post burn (unpaired *t*-test, $p = 0.3039$). That is, skin thickness did not change over the longer time frame. There was also no difference in skin thickness between control and membrane treated samples at either day 56 (4.63 ± 0.43 mm vs. 5.18 ± 0.46 mm respectively; paired *t* test, $p = 0.1979$) or day 70 (4.66 ± 0.16 mm vs. 4.45 ± 0.13 mm respectively; paired *t*-test, $p = 0.3452$) (Fig. 6B).

Epidermal thickness

Histological examination of H&E and MT-stained sections also found that, regardless of the day euthanized, the epidermis from both control and membrane treated wounds was significantly thicker than normal, uninjured skin (47.12 ± 3.92 μm; unpaired *t*-tests, $p < 0.05$) (Fig. 6C). In addition, there was a significant difference in the average epidermal thickness between day 56 (264.12 ± 26.61 μm) and day 70 (128.57 ± 14.49 μm) post burn, with thinner epidermal layers at the later time-point (unpaired *t*-test, $p = 0.0005$). This reduction in thickness is indicative of a more mature epidermal layer as it returns to normal physiological conditions from its hyperproliferative state. For animals euthanized at

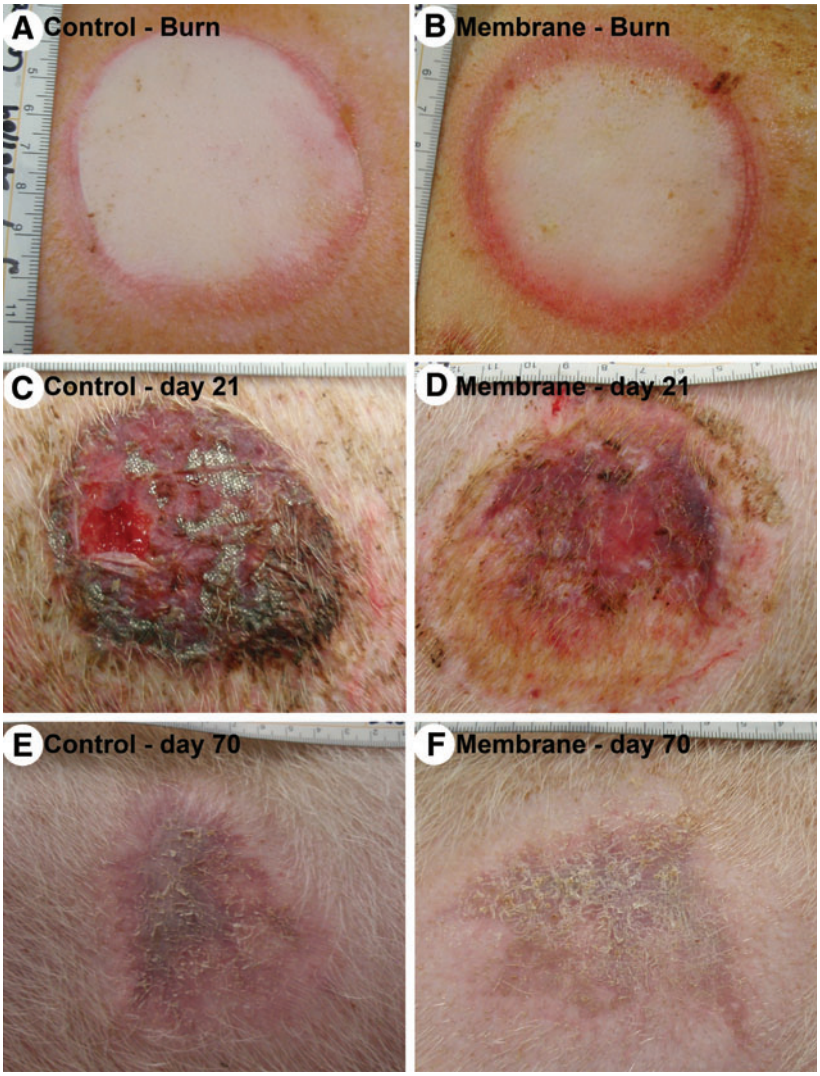

FIG. 4. Gross morphology of wound healing. **(A, C, E)** Digital photographs of a control treated wound at time of burn injury and day 21 and day 70 post burn respectively. **(B, D, F)** Matched membrane treated wound at corresponding time-points. Color images available online at www.liebertonline.com/tea

day 56 post burn, there was no significant difference in epidermal thickness between control (259.43 ± 42.98 μm) and membrane (268.81 ± 37.99 μm) treatments (paired *t*-test, $p = 0.7076$). However, for animals euthanized at day 70 post burn, the epidermis was significantly thicker in control wounds (141.62 ± 21.03 μm) compared to nano-membrane treated wounds (115.52 ± 20.60 μm) (paired *t*-test, $p = 0.0380$) (Fig. 6C). This result suggests an advanced restoration of epidermal maturation when wounds were covered with nano-membranes compared to standard dressings.

Organizing granulation tissue

The amount of organizing granulation tissue (OGT) was also measured in each section.[14] Histological assessment for OGT in the biopsies at day 42, and then in wounds at day 56

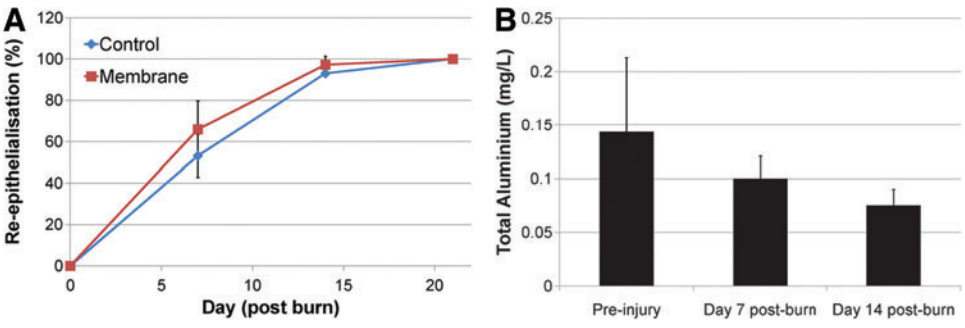

FIG. 5. **(A)** Average re-epithelialization (% of original wound area) for control and membrane treated wounds (data points are mean ± SE). There was no significant difference between treatments ($p > 0.05$). **(B)** Total aluminum content in blood plasma collected pre-injury and days 7 and 14 post burn. There was no difference in aluminum concentration after contact with the nanoporous membrane. Color images available online at www.liebertonline.com/tea

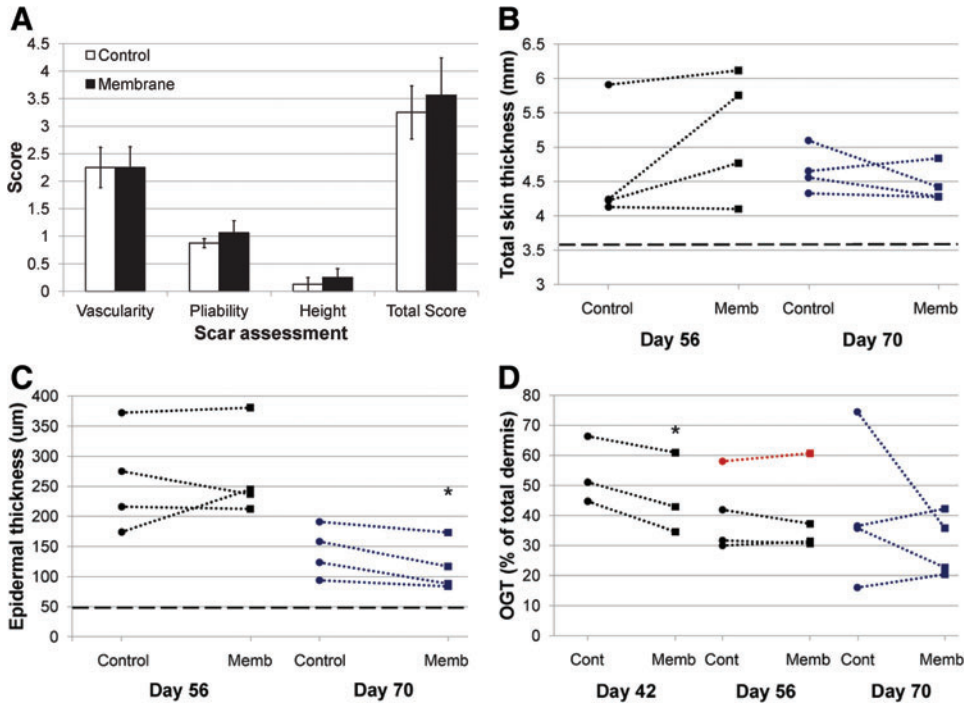

FIG. 6. Effect of 300 nm nanoporous membrane dressing on porcine wounds. **(A)** There was no significant difference in the gross clinical assessments of the final scars between control and membrane treated wounds. **(B)** Total skin thickness. Regardless of the day euthanized (day 56 or day 70) there was no significant difference in the total skin thickness between control and membrane treated wounds. **(C)** Epidermal thickness. For animals euthanized day 56 post burn there was no significant difference between treatments, but for animals euthanized day 70 post burn, membrane treated wounds had a significantly thinner epidermis (*paired *t*-test; $p = 0.0380$). The epidermal thickness decreased over time. **(D)** Organizing granulation tissue. There was significantly less organizing granulation tissue organizing granulation tissue (OGT) in membrane treated wounds compared to control wounds at an earlier time-point (day 42; *paired *t*-test, $p = 0.0283$). There was no significant difference between treatments at day 56 or day 70. The amount of OGT decreased over time. For each of the histological analyses, the data presented is the paired data of control and test wounds from each individual pig ($n = 4$ euthanized at day 56; $n = 4$ euthanized at day 70. Each data point is averaged from the 6 sections collected and analyzed from both anteroposterior and dorsoventral axes through the wound). The broken line (· · · · · · · ·) represents the thickness of normal skin. Color images available online at www.liebertonline.com/tea

showed, as expected, a significant decrease in the amount of OGT with time (control day 42; 54.1 ± 6.4% vs. control day 56; 34.5 ± 3.7%; paired *t*-test, $p = 0.0290$. Membrane day 42; 46.1 ± 7.8% vs. membrane day 56; 33.1 ± 2.1%; paired *t*-test, $p = 0.1509$) (Fig. 6D). Further analysis of OGT at day 42 post burn showed that wounds covered with nanoporous membranes had significantly less OGT than the control treated wounds (46.1 ± 7.8% vs. 54.1 ± 6.4% respectively; paired *t*-test, $p = 0.0283$) (Fig. 6D). By day 56, there was no significant difference between control (40.4 ± 6.4%) and membrane (40.0 ± 7.1%) treated wounds (paired *t*-test, $p = 0.8127$). Similarly, for animals euthanized at day 70 post burn, there was no significant difference in the amount of OGT in the final scars (control; 40.7 ± 12.2% vs. membrane; 30.3 ± 5.2%; paired *t*-test, $p = 0.3894$) (Fig. 6D).

Discussion

AAO membranes as cell culture substrates

Nanoporous AAO membranes were model substrates for the study. Aluminum oxide has long been appreciated for its biocompatibility in the human body[22] and has current applications in orthopedic prostheses and dental implants.[23,24] The highly regular architecture was stable in cell culture, with no adverse reactions or infections or observation of membrane breakdown over the length of the culture periods. SEM analysis also showed that the pores were not clogged by the cells or the cell culture medium. AAO membranes have also been used as nanostructured substrates for a number of different cell types. Osteoblast,[25] neutrophil,[26] hepatoma,[27] and marrow stromal[28] cell types have all been cultured on AAO membranes with demonstrated attachment, proliferation and production of ECM proteins. Here we have used AAO as a template for culture of skin derived cells (specifically keratinocytes) and as demonstrated with other cell types, keratinocytes attached, proliferated, and were viable over a long period of time on the nanoporous alumina surfaces.

Nanotopography affects cell morphology and proliferation

The shape of the cell was affected by the nanoporous topography of the AAO template. The majority of cells on the 41 nm, 58 nm, and 114 nm membranes had a more rounded morphology, while cells on the 300 nm membrane and the control were better spread and flat. In support of the current findings, previous studies have shown that cells cultured on nanostructured substrates tended to have more rounded cell morphology.[11,12,29–32] The shape of a cell is closely linked to cell function. Cells produce distinct morphologies when motile and when entering the S-phase of the cell cycle for mitosis. Motile cells tend to have a rounded cell body with a leading edge and many filopodia. Static cells, however, are normally well spread with many contractile stress fibers pulling the cells flat from large, established focal adhesions.[31,33] For anchorage-dependent

cells, spreading is a prerequisite for cells to enter the S or DNA replication phase of cell division.[34] Therefore, it can be concluded that keratinocytes on the 41 nm, 58 nm, and 114 nm membrane cells were displaying a more migratory cell phenotype, while cells on the 300 nm membrane and control had a greater capacity for proliferation. This was reflected in the proliferation data, with slower proliferation observed on the smaller sized membranes, and faster proliferation observed on the 300 nm and control surfaces. Previous studies have reported the same phenomena. Differences in fibroblast morphology on 13 nm, 35 nm, and 95 nm islands were complemented with differences in proliferation.[30] Furthermore, while fibroblasts were seen to interact quickly and strongly with nanocolumns (160 nm high, 100 nm wide), they were also reported to grow less well on these nanopatterned surfaces.[35] It was suggested the cells remained motile on the surface instead of settling down to make strong contacts with the material as they did with the flat surfaces and was confirmed with the observation of distinct differences in focal adhesion morphology on the nanostructured surfaces. Taken together with the results in this study, cells tend to have a round motile morphology on smaller nanostructured surfaces, producing many filopodia to explore and probe the environment surrounding the cell. Since cell spreading is a requirement for cell division, proliferation was slower on these substrates.

Nanotopography affects cell migration

Keratinocytes were very motile on the nanostructured membranes, with an increase in cell migration with increasing pore size. Cells initially migrated faster across all the membranes tested (41 nm, 58 nm, 300 nm) compared to the flat control. This included the 300 nm membrane, which supported the fastest cell migration overall. This membrane appeared to support both proliferative and migratory cell phenotypes. The presence of the nanoporous topography was likely to enhance the migration. Previous studies have shown the migration of corneal epithelial tissue onto various polymers was stimulated one and a half- to threefold by the presence of 100 nm pores compared to that on equivalent nonporous materials.[36] The surface chemistries were also altered, and it was reported that even for the most stimulatory surface chemistry (such as covalently attached collagen), migration over the surface was suboptimal if the material was nonporous. The presence of pores appeared to unlock further tissue migratory potential for all but the least supportive surface chemistries.[36] Further to this work, corneal epithelial cell migration across polymers surfaces with randomly arranged 100 nm and 400 nm pores showed a one and a half and twofold increase in migration respectively.[37] As observed on the AAO membranes, there was an increase in cell migration with increasing pore size. To further support the claims that the differences in migration were due to nanoscale changes in topography the same group showed that blind-ending the pores (to abolish any potential effect of fluid flux through the membrane) did not affect the level of enhancement on the 100 nm and 400 nm pores.[37] The study showed that the increased rate of migration on surfaces that contained pores was a response to the topography rather than the porosity. The same reasoning can be applied to the results in this work, since membranes were adhered to the bottom of culture wells.

The effects of the 300 nm AAO membrane on wound healing in vivo

A deep dermal partial thickness (DDPT) burn model in the pig[14] was used to analyze the effect of the 300 nm nanoporous AAO membrane on wound repair after burn injury. A DDPT burn model was selected as these burns are the most common depth of injury presenting to pediatric hospitals and are the most difficult to manage.[20,38,39] On each animal, one wound was dressed directly with the 300 nm membrane (with Acticoat as a secondary dressing) and the other with Acticoat; a standard burns dressing. Acticoat is a nanocrystalline silver dressing and was selected as the control dressing for this study as it is the most commonly applied wound dressing in our burns center and has many reported advantages as a wound dressing.[40] It has also been used as the primary dressing in other reports using the same porcine model.[20,41] The nano-membrane was applied to act as an interactive dressing to potentially exploit the favorable cell processes observed with keratinocytes *in vitro* and enhance wound repair for improved outcome, in particular to speed up the wound healing process, which is known to lead to better aesthetic and functional outcomes.[42]

An ideal wound dressing should have several key attributes. The dressing should protect the wound from bacterial infection, keep a moist environment while still allowing permeability of oxygen and carbon dioxide, and enhance healing.[43–45] Additionally, it should be composed of materials that are nontoxic, nonimmunogenic, flexible, and durable.[43] An important finding in this work was that the nano-membrane (together with the secondary dressings) created a wound-healing environment that appeared to provide for these conditions. First, no signs of bacterial infection were apparent during gross examination of the wounds or from the biopsies collected during wound healing, indicating that if the standard wound dressing procedures are used (i.e., dressing wounds with the autoclaved AAO membranes in conjunction with Acticoat) it is unlikely that infection will occur. Secondly, the wounds treated with the membranes appeared moist, demonstrating that wound dehydration had been prevented. Third, wounds healed with abundant cellular proliferation and migration similar to the control, suggesting oxygen and carbon dioxide permeability had been maintained. Finally, treatment with the AAO membranes indicated an enhancement of the overall wound healing process with less OGT and more mature epidermal layers at earlier time-points.

The membranes conformed well to the pig flank and were stable within the wound environment with no observed degradation. Blood samples indicated that there was no systemic adsorption of aluminum from the membranes. The observation of less OGT earlier in wounds dressed with the membrane further supports conclusions about the stability and biocompatibility of the membrane material in the wound environment, as any degradation would likely induce new inflammatory responses against the degraded fragments and result in more OGT.[46] Similarly, if the membrane was rejected due to noncompatibility, there would have been a large inflammatory response and delayed healing. AAO membranes are also synthetic, inorganic dressings that do

not have the inherent risk of transmitting disease that other biological dressings and transfer membranes have. These observations, along with the evidence of advanced healing, further support the application of AAO membranes in wound healing.

Despite the potential to influence the rate of wound closure by enhanced migration, gross observations of re-epithelialization did not show any significant differences between control and membrane covered wounds. However, histological assessment of the final scars showed enhanced wound healing and maturity of membrane treated wounds compared to control wounds, suggesting differences in healing that may not have been observed from gross observations. A statistically significant decrease in OGT was observed in membrane treated wounds at day 42 post burn. OGT, also known as the scar tissue layer[47] or wound inflammatory layer,[48] consists of proliferating fibroblasts and capillaries and initially has a loose structure that organizes with time to form a dense scar. It is believed that the amount of OGT in a wound is indicative of the extent of later scarring.[14] That is, the more OGT that is produced, the more tissue will need to be remodeled at a later date, ultimately leading to more burn scar. It follows that treatments which limit the amount of OGT formation could potentially minimize the future scar and improve the outcome.[48] Significantly less OGT was observed in membrane treated wounds, indicating that these wounds either had formed less OGT overall, or that they were recovering and organizing faster to result in less cellular tissue and more mature scars.

In the final scars, at day 56 and day 70 post burn, there was no difference in the amount of OGT in control and membrane treated wounds. If the amount of OGT is an indication of the appearance of the future scar as previously reported,[14,48] these results support the clinical assessments of the final scars. It follows that in observing less OGT at an earlier time-point, wounds dressed with the membrane were organizing faster to result in less cellular granulation tissue. However, within the extended timeframe of healing, control wounds were able to catch up and organize to be similar to the membrane wounds. This phenomenon has been seen with other wound healing studies, demonstrating early improvements in healing with first aid or debridement after injury, but ultimately similar outcomes with control samples.[49,50] The evaluation of glycosaminoglycan (GAG) hydrogel films as bio-interactive dressings in a full thickness, excisional mouse model also showed similar end points of re-epithelialization between control and test wounds despite an earlier increase with the GAG dressings.[43] The fact that outcomes are similar is likely to be a result of the increased healing ability of all animal models when compared to humans, and the data from earlier time-points suggesting more rapid healing provide a strong indication that the use of the AAO membrane would improve outcomes in patients when compared to the standard dressing. Further, epidermal layers in the final scars were also more mature in membrane treated wounds compared to control wounds, which is indicative of a faster wound healing process.

Further application

While wounds dressed with the nanoporous membrane had less OGT at an earlier time-point and more mature epidermal layers when compared to control wounds, these desirable wound healing characteristics did not impact on the gross morphology and clinical outcome of the scars in this porcine model. While this may translate differently in humans, it is postulated that final scar outcome may be further improved by exploiting the enhanced healing with other scar management therapies to continue to drive the repair. For example, many authors report the use of silicone materials[51] and pressure therapy[52] for the conservative management of scars, for their likely influence on the collagen remodeling phase of wound healing.[53] Therefore, if applied after treatment with the nanoporous membrane, these therapies may continue to drive the advanced maturation observed in this work for a better cosmetic outcome. There is also potential to combine established wound healing therapies with the nanoporous membrane to provide a superior topographical and physicochemical approach to wound healing. For example, substrate-bound vitronectin (VN): growth factor complexes have been shown to stimulate keratinocyte proliferation and migration[54,55] and increase re-epithelialization of DDPT burn injuries *in vivo*.[20] Taken together, keratinocyte function may be further stimulated to drive repair by a membrane functionalized with the complexes. Other therapies such as the antiscarring agent transforming growth factor β3 (TGFβ3)[56] could also potentially combine with the nanoporous membrane for a potent wound healing therapy. Furthermore, there is potential to use nanoporous AAO membranes as a delivery device for the transfer of cultured autologous cells to the wound bed; a concept which has been previously reported with other surfaces with promising results.[46,57]

Conclusion

This research has shown the importance of nano-scale topography in modulating keratinocyte phenotype and wound healing following a burn injury. Differences in keratinocyte morphology, proliferation, and migration were observed due to changes in nanotopography. Application of an AAO membrane with a 300 nm pore size to a partial thickness burn injury in the pig showed improved wound healing at earlier time points. The AAO membrane also performed well as an interactive dressing, with no evidence of degradation in the wound environment and no adverse effect on the wound healing process. Importantly, the research has demonstrated an effect of nanotopography on keratinocyte phenotype and wound healing, and thus need to consider nanoarchitecture in future wound healing therapies.

Acknowledgments

The authors wish to acknowledge Dr. Gerard Eddy Poinern for advice on nanoporous membrane fabrication, Dr. Griet Haitjema and Dr. Chris Quinn for consulting on the anesthesia for the animal work, Professor Max Bulsara and Dr. Hilary Wallace for statistical help and advice, Ms. Astrid Armitage and Mr. Andy Wilson for assistance in the animal house, Mrs. Kerry Parkinson for the creation of the porcine protective jackets, and the Marine and Freshwater Research Laboratory at Murdoch University for the analysis of the bloods. This work was supported by NHMRC development grant 572734.

Disclosure Statement

No competing financial interests exist.

References

1. Chou, L., Firth, J.D., Uitto, V.-J., and Brunette, D.M. Substratum surface topography alters cell shape and regulates fibronectin mRNA level, mRNA stability, secretion and assembly in human fibroblasts. J Cell Sci. 108, **1563,** 1995.
2. Curtis, A., and Wilkinson, C. Topographical control of cells. Biomaterials **18**, 1573, 1997.
3. Zeltinger, J., Sherwood, J.K., Graham, D.A., Mueller, R., and Griffith, L.G. Effect of pore size and void fraction on cellular adhesion, proliferation, and matrix deposition. Tissue Eng **7,** 557, 2001.
4. O'Brien, F.J., Harley, B.A., Yannas, I.V., and Gibson, L.J. The effect of pore size on cell adhesion in collagen-GAG scaffolds. Biomaterials **26,** 433, 2005.
5. McMillan, J.R., Akiyama, M., Tanaka, M., Yamamoto, S., Goto, M., Abe, R., Sawamura, D., Shimomura, M., and Shimizu, H. Small-diameter porous poly (epsilon-caprolactone) films enhance adhesion and growth of human cultured epidermal keratinocyte and dermal fibroblast cells. Tissue Eng **13,** 789, 2007.
6. Clark, P., Connolly, P., Curtis, A.S.G., Dow, J.A.T., and Wilkinson, C.D.W. Cell guidance by ultrafine topography in vitro. J Cell Sci **99,** 73, 1991.
7. Flemming, R.G., Murphy, C.J., Abrams, G.A., Goodman, S.L., and Nealey, P.F. Effects of synthetic micro- and nano-structured surfaces on cell behaviour. Biomaterials **20,** 573, 1999.
8. Teixeira, A.I., Abrams, G.A., Bertics, P.J., Murphy, C.J., and Nealey, P.F. Epithelial contact guidance on well-defined micro- and nanostructured substrates. J Cell Sci **116,** 1881, 2003.
9. Dalby, M.J., Pasqui, D., and Affrossman, S. Cell response to nano-islands produced by polymer demixing: a brief review. IEE Proc Nanobiotechnol **151,** 53, 2004.
10. Park, J., Bauer, S., Schlegel, K.A., Neukam, F.W., von der Mark, K., and Schmuki, P. TiO2 nanotube surfaces: 15 nm—An optimal length scale of surface topography for cell adhesion and differentiation. Small **5,** 666, 2009.
11. Csaderova, L., Martines, E., Seunarine, K., Gadegaard, N., Wilkinson, C.D.W., and Riehle, M.O. A biodegradable and biocompatible regular nanopattern for large-scale selective cell growth. Small **6,** 2755, 2010.
12. Hu, W., Crouch, A.S., Miller, D., Aryal, M., and Luebke, K.J. Inhibited cell spreading on polystyrene nanopillars fabricated by nanoimprinting and in situ elongation. Nanotechnology **21,** 385301, 2010.
13. Parkinson, L.G., Giles, N.L., Adcroft, K.F., Fear, M.W., Wood, F.M., and Poinern, G.E. The potential of nanoporous anodic aluminium oxide membranes to influence skin wound repair. Tissue Eng Part A **15,** 3753, 2009.
14. Cuttle, L., Kempf, M., Phillips, G.E., Mill, J., Hayes, M.T., Fraser, J.F., Wang, X.-Q., and Kimble, R.M. A porcine deep dermal partial thickness burn model with hypertrophic scarring. Burns **32,** 806, 2006.
15. Hernandez, F., and Guillen, R. Microwave Processing for Scanning Electron Microscopy. Eur J Morphol **38,** 109, 2000.
16. Schroeder, J.A., Gelderblom, H.R., Hauroeder, B., Schmetz, C., Milios, J., and Hofstaedter, F. Microwave-assisted tissue processing for same-day EM-diagnosis of potential bioterrorism and clinical samples. Micron **37,** 577, 2006.
17. Promega. Cell Titre 96(R) AQueous One Solution Cell Proliferation Assay. Technical Bulletin Part #TB245, www.promega.com, 2005.
18. Rasband, W. Image J 1.40g, National Institutes of Health, USA. http://rsb.info.nih.gov/ij/, Java 1.6.0_05.
19. Sullivan, T., Smith, J., Kermode, J., McLver, E., and Courtemanche, D.J. Rating the Burn Scar J Burn Care Res **11,** 256, 1990.
20. Upton, Z., Cuttle, L., Noble, A., Kempf, M., Topping, G., Malda, J., Xie, Y., Mill, J., Harkin, D.G., Kravchuk, O., Leavesley, D.I., and Kimble, R.M. Vitronectin: Growth Factor Complexes Hold Potential as a Wound Therapy Approach J Invest Dermatol **128,** 1535, 2008.
21. Cnaan, A., Laird, N.M., and Slasor, P. Using the general linear mixed model to analyse unbalanced repeated measures and longitudinal data. Stat Med **16,** 2349, 1997.
22. Hamadouche, M., Boutin, P., Daussange, J., Bolander, M.E., and Sedel, L. Alumina-on-alumina total hip arthroplasty: a minimum 18.5-year follow-up study. J Bone J Surg **84,** 69, 2002.
23. Langer, R., and Vacanti, J.P. Tissue engineering. Science **260,** 920, 1993.
24. Shackelford, J.F. Bioceramics: current status and future trends. Mater Sci Forum **293,** 99, 1999.
25. Swan, E.E.L., Popat, K.C., Grimes, C.A., and Desai, T.A. Fabrication and evaluation of nanoporous alumina membranes for osteoblast culture. Wiley Periodicals **288,** 2005.
26. Karlsson, M., Johansson, A., Tang, L., and Boman, M. Nanoporous aluminum oxide affects neutrophil behaviour. Microsc Res Tech **63,** 259, 2004.
27. Hoess, A., Teuscher, N., Thormann, A., Aurich, H., and Heilmann, A. Cultivation of hepatoma cell line HepG2 on nanoporous aluminum oxide membranes. Acta Biomater **3,** 43, 2007.
28. Popat, K.C., Chatvanichkul, K.I., Barnes, G.L., Latempa, T.J., Jr., Grimes, C.A., and Desai, T.A. Osteogenic differentiation of marrow stromal cells cultured on nanoporous alumina surfaces. J Biomed Mater Res A **80,** 955, 2007.
29. Andersson, A.-S., Backhed, F., von Euler, A., Richter-Dahlfors, A., Sutherland, D., and Kasemo, B. Nanoscale features influence epithelial cell morphology and cytokine production. Biomaterials **24,** 3427, 2003.
30. Dalby, M.J., Riehle, M.O., Johnstone, H.J., Affrossman, S., and Curtis, A.S. Polymer-demixed nanotopography: control of fibroblast spreading and proliferation. Tissue Eng **8,** 1099, 2002.
31. Dalby, M.J., Riehle, M.O., Sutherland, D.S., Agheli, H., and Curtis, A.S.G. Changes in fibroblast morphology in response to nano-columns produced by colloidal lithography. Biomaterials **25,** 5415, 2004.
32. Krasteva, N., Seifert, B., Albrecht, W., Weigel, T., Schossig, M., Altankov, G., and Groth, T. Influence of polymer membrane porosity on C3A hepatoblastoma cell adhesive interaction and function. Biomaterials **25,** 2467, 2004.
33. Burridge, K., and Chrzanowska-Wodnicka, M. Focal adhesions, contractility, and signaling. Annu Rev Cell Dev Biol **12,** 463, 1996.
34. Folkman, J., and Moscona, A. Role of cell shape in growth control. Nature **273,** 345, 1978.
35. Dalby, M.J., Riehle, M.O., Sutherland, D.S., Agheli, H., and Curtis, A.S.G. Fibroblast response to a controlled nanoenvironment produced by colloidal lithography. J Biomed Mater Res A **69A,** 314, 2004.
36. Steele, J.G., Johnson, G., McLean, K.M., Beumer, G.J., and Griesser, H.J. Effect of porosity and surface hydrophilicity

on migration of epithelial tissue over synthetic polymer. J Biomed Mater Res **50,** 475, 2000.
37. Dalton, B.A., McFarland, G.A., and Steele, J.G. Stimulation of epithelial tissue migration by certain porous topographies is independent of fluid flux. J Biomed Mater Res **56,** 83, 2001.
38. Burd, A., and Yuen, C. A global study of hospitalized paediatric burn patients. Burns **31,** 432, 2005.
39. Gibran, N.S., Boyce, S., and Greenhalgh, D.G. Cutaneous wound healing. J Burn Care Res **28,** 577, 2007.
40. Fong, J., and Wood, F. Nanocrystalline silver dressings in wound management: a review. Int J Nanomedicine **1,** 441, 2006.
41. Wang, X.-Q., Liu, P.-Y., Kempf, M., Cuttle, L., Chang, A.H.-E., Wong, M., Kravchuk, O., Mill, J., and Kimble, R.M. Burn healing is dependent on burn site: a quantitative analysis from a porcine burn model. Burns **35,** 264, 2009.
42. Deitch, E.A., Wheelahan, T.M., Rose, M.P., Clothier, J., and Cotter, J. Hypertrophic burn scars: analysis of variables. J Trauma **23,** 895, 1983.
43. Kirker, K.R., Luo, Y., Nielson, J.H., Shelby, J., and Prestwich, G.D. Glycosaminoglycan hydrogel films as bio-interactive dressings for wound healing. Biomaterials **23,** 3661, 2002.
44. Morin, R.J., and Tomaselli, N.L. Interactive dressings and topical agents. Clin Plast Surg **34,** 643, 2007.
45. Boateng, J.S., Matthews, K.H., Stevens, H.N.E., and Eccleston, G.M. Wound healing dressings and drug delivery systems: a review. J Pharm Sci **97,** 2892, 2008.
46. Van Den Bogaerdt, A.J., Ulrich, M.M.W., Van Galen, M.J.M., Reijnen, L., Verkerk, M., Pieper, J., Lamme, E.N., and Middelkoop, E. Upside-down transfer of porcine keratinocytes from a porous, synthetic dressing to experimental full-thickness wounds. Wound Repair Regen **12,** 225, 2004.
47. Zhu, K.Q., Engrav, L.H., Gibran, N.S., Cole, J.K., Matsumura, H., Piepkorn, M., Isik, F.F., Carrougher, G.J., Muangman, P.M., Yunusov, M.Y., and Yang, T.-M. The female, red Duroc pig as an animal model of hypertrophic scarring and the potential role of the cones of skin. Burns **29,** 649, 2003.
48. Harunari, N., Zhu, K.Q., Armendariz, R.T., Deubner, H., Muangman, P., Carrougher, G.J., Isik, F.F., Gibran, N.S., and Engrav, L.H. Histology of the thick scar on the female, red Duroc pig: final similarities to human hypertrophic scar. Burns **32,** 669, 2006.
49. Cuttle, L., Kempf, M., Kravchuk, O., Phillips, G.E., Mill, J., Wang, X.Q., and Kimble, R.M. The optimal temperature of first aid treatment for partial thickness burn injuries. Wound Repair Regen **16,** 626, 2008.
50. Wang, X.Q., Kempf, M., Liu, P.Y., Cuttle, L., Chang, H.E., Kravchuk, O., Mill, J., Phillips, G.E., and Kimble, R.M. Conservative surgical debridement as a burn treatment: Supporting evidence from a porcine burn model. Wound Repair Regen **16,** 774, 2008.
51. Ahn, S.T., Monafo, W.W., and Mustoe, T.A. Topical silicone gel for the prevention and treatment of hypertrophic scar. Arch Surg **126,** 499, 1991.
52. Van den Kerckhove, E., Stappaerts, K., Fieuws, S., Laperre, J., Massage, P., Flour, M., and Boeckx, W. The assessment of erythema and thickness on burn related scars during pressure garment therapy as a preventive measure for hypertrophic scarring. Burns **31,** 696, 2005.
53. Bloemen, M.C.T., van der Veer, W.M., Ulrich, M.M.W., van Zuijlen, P.P.M., Niessen, F.B., and Middelkoop, E. Prevention and curative management of hypertrophic scar formation. Burns **35,** 463, 2009.
54. Hyde, C., Hollier, B., Anderson, A., Harkin, D., and Upton, Z. Insulin-like growth factors (IGF) and IGF-binding proteins bound to vitronectin enhance keratinocyte protein synthesis and migration. J Invest Dermatol **122,** 1198, 2004.
55. Hollier, B., Harkin, D.G., Leavesley, D., and Upton, Z. Responses of keratinocytes to substrate-bound vitronectin:-growth factor complexes. Exp Cell Res **305,** 221, 2005.
56. Ferguson, M.W., Duncan, J., Bond, J., Bush, J., Durani, P., So, K., Taylor, L., Chantrey, J., Mason, T., James, G., Laverty, H., Occleston, N.L., Sattar, A., Ludlow, A., and O'Kane, S. Prophylactic administration of avotermin for improvement of skin scarring: three double-blind, placebo-controlled, phase I/II studies. Lancet **373,** 1264, 2009.
57. Chester, D.L., Balderson, D.S., and Papini, R.P. A review of keratinocyte delivery to the wound bed. J Burn Care Rehabil **25,** 266, 2004.

Address correspondence to:
Leigh G. Parkinson, Ph.D.
McComb Research Foundation/Burn Injury Repair Unit, School of Surgery
The University of Western Australia
M318, 35 Stirling Highway
Crawley, WA 6009

E-mail: leighgparkinson@gmail.com

Received: May 27, 2011
Accepted: October 10, 2011
Online Publication Date: December 5, 2011